Monthly Notices
of the
ROYAL ASTRONOMICAL SOCIETY

MNRAS **479,** 153–161 (2018)
Advance Access publication 2018 June 07

doi:10.1093/mnras/sty1481

Cosmic ray heating of intergalactic medium: patchy or uniform?

Ranita Jana★ and Biman B. Nath
Raman Research Institute, Sadashiva Nagar, Bangalore 560080, India

Accepted 2018 June 1. Received 2018 June 1; in original form 2017 December 5

ABSTRACT

We study the heating of the intergalactic medium (IGM) surrounding high redshift star-forming galaxies due to cosmic rays (CR). We take into account the diffusion of low-energy CR and study the patchiness of the resulting heating. We discuss the case of IGM heating around a high redshift minihalo ($z \sim 10$–20, M $\sim 10^5$–10^7 M$_\odot$) and put an upper limit on the diffusion coefficient $D \leq 1 \times 10^{26}$ cm^2 s^{-1} for the heating to be inhomogeneous at $z \sim 10$ and $D \leq 5$–6×10^{26} cm^2 s^{-1} at $z \sim 20$. For typical values of D, our results suggest uniform heating by CR at high redshift, although there are uncertainties in magnetic field and other CR parameters. We also discuss two cases with continuous star formation, one in which the star formation rate (SFR) of a galaxy is high enough to make the IGM in the vicinity photoionized, and another in which the SFR is low enough to keep it neutral but high enough to cause significant heating by CR protons. In the neutral case (low SFR), we find that the resulting heating can make the gas hotter than the cosmic microwave background radiation for $D < 10^{30}$ cm^2 s^{-1}, within a few kpc of the galaxy, and unlikely to be probed by near future radio observations. In the case of photoionized IGM (high SFR), the resulting heating of the gas in the vicinity of high redshift ($z \sim 4$) galaxies of mass $\geq 10^{12}$ M$_\odot$ can suppress gas infall into the galaxy. At lower redshifts ($z \sim 0$), an SFR of $\sim$1 M$_\odot$ yr^{-1} can suppress the infall into galaxies of mass $\leq 10^{10}$ M$_\odot$.

Key words: supernovae: general – cosmic rays – intergalactic medium – dark ages, reionization, first stars.

1 INTRODUCTION

Galaxies interact with the surrounding gas in various ways, through gravitational and mechanical means as well as through radiation. The gravitational field of collapsed structures help them to accrete matter from surrounding regions, setting up an inflow of gas and dark matter. The radiation emanating from stars and possible active galactic nuclei (AGN) also affect the intergalactic medium (IGM), by ionizing and heating. The process of star formation and AGN activities stir up the interstellar medium (ISM) of the galaxies, often setting up galactic outflows that interact with the IGM gas through fluid dynamical interactions. There is yet another type of interaction that has been discussed in the literature, through high-energy particles, that may be produced during the star formation or AGN activity in galaxies.

Ginzburg & Ozernoy (1966) pointed out that cosmic rays (CR) accelerated in supernovae (SNe) and radio galaxies could raise the temperature of the IGM gas to $\geq 10^5$ K. Their argument was based on the fact that low-energy CRs lose a large fraction of their energy through Coulomb interactions. Nath & Biermann (1993) addressed the question of possible reionization of the Universe through such processes and concluded that it would require a very large star formation rate (SFR) density. According to Lacki (2015), CRs would contribute towards a significant non-thermal pressure of the IGM gas. Another possible effect of CRs in the IGM discussed in the literature is the production of ^6Li by CR α particles. Nath, Madau & Silk (2006) showed the observed abundance ratio of $^6Li/H$ can be related to the observed entropy of the intracluster medium, through Coulomb heating.

Recently, Sazonov & Sunyaev (2015) suggested that low-energy CRs (with kinetic energy $\leq$30 MeV per nucleon) could have heated the neutral IGM at high redshift and change the HI emission characteristics of the gas. Such a feature can be potentially detected in planned experiments that will detect redshifted 21 cm emission. Following this argument, Leite et al. (2017) calculated in detail the heating of the IGM by CRs and found that the IGM temperature could have been increased by $\Delta T \sim 100$ K at $z \sim 10$.

However, as Leite et al. (2017) and others have pointed out, the propagation of the CRs crucially depend on the diffusion coefficient. Diffusion of CRs can heat the surrounding gas in a non-uniform manner. In this paper, we discuss the heating of IGM by CRs produced by star- forming galaxies, as a function of diffusion coefficient, gas density, SFR, and other relevant parameters and discuss the implication of this kind of heating.

★ E-mail: ranita@rri.res.in

2 PRELIMINARIES

We consider the heating effect of CR protons in this paper on the IGM gas surrounding a galaxy. The energy deposition by protons depends on several parameters, and next, we list our assumptions regarding them.

2.1 CR spectrum

The CR luminosity of a galaxy is determined by its SFR, assuming a Salpeter initial mass function (with 0.1 $M_\odot$ and 30 $M_\odot$ as the lower and upper limits), with a total mechanical energy output of 10^{51} erg SNe^{-1} and an efficiency of η for CR acceleration. There is a significant uncertainty in this parameter (from less than 0.1 to ~ 0.5). We assume a value of $\eta = 0.1$, which is supported by the simulation results of Caprioli & Spitkovski (2014). This gives us

$$L_{\rm cr} = 2 \times 10^{40}\,{\rm erg\,s^{-1}} \left(\frac{\eta}{0.1}\right)\left(\frac{\rm SFR}{1\,M_\odot\,{\rm yr^{-1}}}\right). \quad (1)$$

We assume that the CR protons leave the galactic virial radius $R_{\rm vir}$, with a spectrum $n_{cr}(p_0) \propto p_0^\alpha$, where $p_0 (\equiv p(r = R_{\rm vir}))$ denotes the momentum of protons as they leave the galaxy at $r = R_{\rm vir}$, and $n_{\rm cr}(p_0)$ is the rate of CRs (number of CR per second) coming out of the galaxy with momentum p_0. In our calculation, we assume $\alpha = -2.5$ and discuss the effect of changing its value later in the paper.

The spectrum is normalized such that the total energy flux corresponds to the above-mentioned CR luminosity, or

$$L_{cr} = \int_{p_{0,\rm min}}^{p_{0,\rm max}} E_{\rm k} n_{cr}(p_0) {\rm d}p_0\,, \quad (2)$$

where $p_{0,\rm min}$ and $p_{0,\rm max}$ are the lower and upper limits of CR momenta, respectively, with kinetic energy $E_{\rm k} = \sqrt{p^2c^2 + m_p^2c^4} - m_pc^2$. By denoting $x_0 = p_0/(m_pc)$, CR spectrum can be written (in terms of number of particles per unit time) as

$$n_{cr}(p_0){\rm d}p_0 = \left(\frac{L_{cr}}{(m_pc^2)(m_pc)^{\alpha+1}\int[\sqrt{1+x_0^2}-1]x_0^\alpha {\rm d}x_0}\right) p_0^\alpha {\rm d}p_0, \quad (3)$$

where the integration is carried out between $x_{0,\rm min} = \frac{p_{0,\rm min}}{m_pc}$ and $x_{0,\rm max} = \frac{p_{0,\rm max}}{m_pc}$. We will find it more convenient to describe the spectrum in terms of $\beta (\equiv v/c)$, and in the rest of the paper, we will write the emergent spectrum from the galaxy in equation (3) as $n_{cr}(\beta_0){\rm d}\beta_0$, where $p_0 = \frac{m_p\beta_0 c}{\sqrt{1-\beta_0^2}}$.

The heating effect of CRs is insensitive to the upper limit of energy but depends strongly on the lower limit since the energy loss rate increases with decreasing CR energy. The previous works by Sazonov & Sunyaev (2015) and Leite et al. (2017) considered heating by protons of $\leq$10–30 MeV. However, protons with very low energy, with $\leq$1 MeV, are unlikely to survive the interactions with the ISM of the parent galaxy for the following reasons. The loss of (kinetic) energy by a proton through interaction with ionized gas of electron density n_e cm^{-3} and temperature T_e K is given by (Mannheim & Schlickeiser 1994, their equation 4.22)

$$-\frac{{\rm d}E_{\rm k}}{{\rm d}t} \approx 5 \times 10^{-19}\,{\rm erg\,s^{-1}} \left(\frac{n_e}{\rm cm^{-3}}\right)\frac{\beta^2}{x_m^3+\beta^3}\,, \quad (4)$$

where $x_m = 0.0286(T_e/2 \times 10^6\,{\rm K})^{1/2}$.

For a CR proton in a neutral medium with particle density $n_{\rm HI}$, the energy loss rate is given by equation (4.32) of Mannheim & Schlickeiser (1994):

$$-\frac{{\rm d}E_{\rm k}}{{\rm d}t} = 3 \times 10^{-19}\,{\rm erg\,s^{-1}} \left(\frac{n_{\rm HI}}{\rm cm^{-3}}\right) \times (1 + 0.0185\,\ln\beta\, H[\beta - \beta_c])\frac{2\beta^2}{\beta_c^3 + 2\beta^3}\,, \quad (5)$$

where $\beta_c \approx 0.01$, corresponding to the orbital speed of electrons in a hydrogen atom. For analytical simplicity, we neglect the term (1 + 0.0185 ln $\beta H[\beta - \beta_c]$) in the above expression since it does not significantly affect the result.

This can be used to estimate the grammage ($\int n_e m_p \beta c {\rm d}t$) required to drain a proton of its kinetic energy (when $E_{\rm k} \approx {\rm d}E_{\rm k}$). We show this value of grammage as a function of proton kinetic energy in Fig. 1. We also superimpose several relevant values of line-of-sight grammage as horizontal lines, corresponding to different galaxy masses at redshift 10, estimated as $\frac{{\rm M_h}\,f_{\rm b}}{R_{\rm vir}(z)^2}$, where $M_{\rm h}$ is the total halo mass of a galaxy, $f_{\rm b} \approx 0.15$ is the cosmic baryon fraction, and $R_{\rm vir}(z)$ is the virial radius at redshift z.

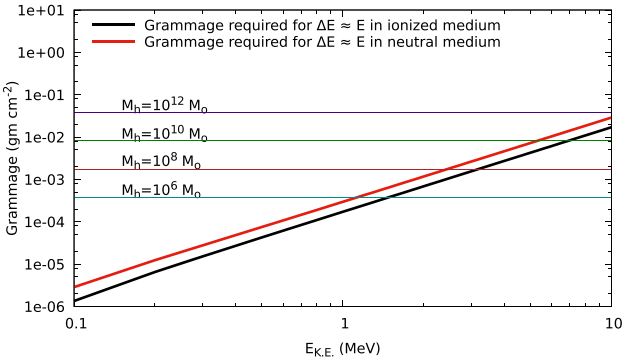

Figure 1. Grammage to deplete the total energy of a proton is shown against the proton kinetic energy for ionized and neutral media. Corresponding line-of-sight grammages for galaxies with $M_{\rm h} = 10^6$, 10^8, 10^{10}, and 10^{12} $M_\odot$ are shown for $z = 10$.

The curves in the figure show that protons of energy less than 0.1–1 MeV are likely to lose all their energy if they were to travel through the ISM of the parent galaxy in a straight path. Therefore, this value should indicate the lower limit of energy, $E_{\rm min}$, corresponding to the lower limit of momentum $p_{0,\rm min}$ mentioned above.

However, there are two possibilities that can change the lower limit. CRs may *diffuse* through the ISM, and the corresponding grammage is likely to be much higher than depicted as horizontal lines here. For example, in the case of Milky Way, the inferred grammage of $\sim$10 g cm^{-2} is much larger than the total column density of the disc and the corresponding $E_{\rm min} \sim 50$ MeV, where a break in CR spectrum is expected and is indeed observed (Nath, Gupta & Biermann 2012).

On the other hand, CRs in star-forming galaxies may be *advected* by gas in the ensuing galactic outflow. In this case, the lower limit of energy may decrease because of adiabatic loss. Since the adiabatic loss of CR energy scales as $\Delta E \propto R^{-1}$, the factor by which the lower limit of energy will decrease is $\epsilon_{\rm adv}$ roughly the ratio of the size of a galaxy halo and the region of CR production, *i.e.* the disc of a star-forming galaxy (Nath & Biermann 1993). This ratio is roughly of order $\sim$0.1, and we adopt this value for $\epsilon_{\rm adv}$.

Therefore, we assume two values of the lower limit of energy, 0.1 and 1 MeV, to encapsulate the uncertainties in the processes of CR propagation until it reaches the IGM.

2.2 CR diffusion

For heating of the gas in which CRs propagate, it is the low-energy CRs that play an important role since the amount of energy lost by a CR increases with decreasing energy. In our context, the energy range of interest is ≤100 MeV, as has been pointed out by previous workers (Sazonov & Sunyaev 2015; Leite et al. 2017).

The diffusion coefficient of CRs is believed to depend on energy, and this dependence in the Milky Way is estimated from a comparison of the observed CR spectrum with what is believed to be the source spectrum. There is, however, considerable uncertainty in the interpretation. Phenomenologically, a few prescriptions for the diffusion coefficient are used in the literature and in models such as GALPROP (see e.g. Ptuskin 2012). In the 'plain diffusion model', the diffusion coefficient for low-energy CR is thought to be $D = 2.2 \times 10^{28} \beta^{-2}$ cm^{2}s^{-1}. As has been pointed out by Ptuskin (2012), the increase in the diffusion coefficient with decreasing energy has no physical explanation and is purely a phenomenological inference. The other common model of diffusion coefficient is that of 'distributed reacceleration', which scales as $p^{1/3}$, and therefore decreases with decreasing energy (see fig. 1 of Ptuskin et al. 2006). Therefore, it is not clear from phenomenological studies if the diffusion coefficient should increase or decrease with decreasing energy at low energies. For simplicity, we assume the diffusion coefficient to be constant for low-energy CR protons.

The diffusion coefficient also depends on the magnetic field because the diffusion of CRs depends on particle scattering by magnetohydrodynamic waves and irregularities. For Kolmogorov-type spectrum of turbulence, the diffusion coefficient for scattering of protons off magnetic irregularities scales as $D \propto r_g^{2-5/3} \propto B^{-1/3}$, where r_g is the gyroradius (Ptuskin 2012).

In light of the above discussion, we assume the diffusion coefficient of low-energy CRs to be constant, to be 2×10^{28} cm^2 s^{-1}, for a 5μG magnetic field in the Milky Way ISM. The present-day IGM magnetic field strength is estimated to be of order ∼10^{-9} G (Subramanian 2016). Using the expected scaling of $D \propto B^{-1/3}$ for Kolmogorov spectrum of magnetic irregularities, we estimate the diffusion coefficient at present epoch to be $D \sim 3 \times 10^{29}$ cm^2 s^{-1}. The magnetic field strength scales with redshift as $B \propto (1+z)^2$ since the magnetic energy density scales as $(1+z)^4$. This implies a value of the diffusion coefficient at $z \sim 10$ to be $D \sim 10^{29}$ cm^2 s^{-1}. We use this as the fiducial value in our calculation for heating of the IGM gas at high redshift ($z \sim$ 10–20). However, we discuss the effect of changing the diffusion coefficient in our results.

2.3 Physical property of IGM near the galaxy

We assume for simplicity a static and uniform density gas around the galaxy, with number density $n_{\rm IGM}$ cm^{-3}. The IGM density near a galaxy is likely to be larger than the critical matter density, and we assume that it is a factor $\Delta \approx 10$ times the critical density at a given epoch. In other words

$$\rho_{\rm IGM}(z) = 10 \times f_b \rho_{cr} \Omega_m(z) = 5.6 \times 10^{-27}\,{\rm cm}^{-3} \left(\frac{\Delta}{10}\right)\left(\frac{1+z}{11}\right)^3. \quad (6)$$

The cosmological parameters used are determined by Planck Collaboration XVI (2015). Therefore, our assumed number density of gas ($n_{\rm IGM} = \frac{\rho_{\rm IGM}}{\mu m_p}$) is 2.8×10^{-3}cm^{-3} in neutral medium ($\mu = 1.2$) and 5.6×10^{-3}cm^{-3} in ionized medium ($\mu = 0.6$) at redshift 10, whereas the number density of electron is 2.9×10^{-3}cm^{-3} since $\mu_e = 1.14$.

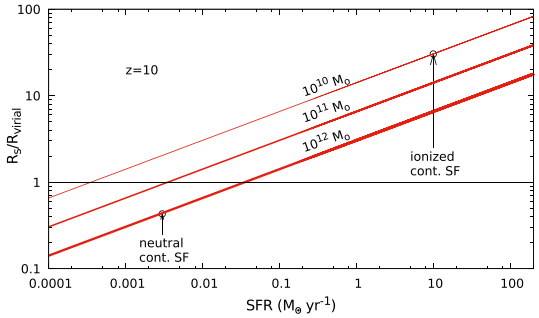

Figure 2. Ratio of Strömgren Sphere radii and virial radii of galaxies of $M_h = 10^{10}$, 10^{11}, and 10^{12} M$_\odot$ are shown as a function of SFR at $z = 10$. Arrow marks show the fiducial SFR chosen for the cases of neutral and ionized IGM.

We will justify our assumption in Section 4.3 by showing that a uniform density with $\Delta = 10$ approximately gives same results as in the case of a density profile that is more realistic outside the halo, within the relevant distance.

The IGM near a galaxy is also likely to be photoionized, owing to the ionizing radiation from massive stars, even before the first SNe begin to produce CR. This can be demonstrated by estimating the Strömgren sphere radius for different values of SFR and Δ. Using STARBURST99, we find that for a continuous star formation scenario, the number of ionizing photons radiated per second is ≈2×10^{54}(SFR/10 M$_\odot$ yr^{-1}) at 10 Myr after the onset of star formation. This gives a Strömgren sphere radius as

$$R_s \approx 193.8\ {\rm kpc} \left(\frac{\rm SFR}{10\,{\rm M}_\odot\,{\rm yr}^{-1}}\right)^{1/3} \left(\frac{\Delta}{10}\right)^{-2/3} \left(\frac{f_b}{0.157}\right)^{-2/3} \times \left(\frac{h}{0.677}\right)^{-4/3} \left(\frac{\Omega_{m,0}}{0.309}\right)^{-2/3} \left(\frac{1+z}{11}\right)^{-2} \quad (7)$$

For $z = 10$, the corresponding radius is ∼ 194 kpc (SFR/10 M$_\odot$ yr^{-1})$^{1/3}$. This length-scale is much larger than the diffusion length of CR particles with $D \sim 10^{29}$ cm^2 s^{-1}, for a time-scale of 100 Myr, the typical duration of a burst of star formation. In other words, the heating effect of CRs is limited to an ionized region, for galaxies with SFR ∼10 M$_\odot$ yr^{-1}. For a smaller SFR, one may have to consider a neutral IGM.

In order to ascertain whether or not the IGM in the vicinity of the galaxy is neutral or ionized, the size of the ionized region can also be compared with the virial radius of a galaxy. We plot in Fig. 2 the ratio of Strömgren radius to virial radius, as a function of SFR, for three different galaxy masses $M_h = 10^{10}$, 10^{11}, and 10^{12} M$_\odot$ at $z = 10$. The lower half region of the figure, with $R_s/R_{\rm vir} \leq 1$ refers to the case of neutral IGM gas in the vicinity of a galaxy. For example, for a galaxy with mass $M_h = 10^{10}$ M$_\odot$ at $z = 10$, SFR has to be $<10^{-3}$ M$_\odot$ yr^{-1} for the gas to be neutral.

Therefore, we consider two cases, one in which the surrounding gas is neutral and another in which it is photoionized. In the neutral case, we assume the gas temperature to be $T = 2.73 \times 151 \times [(1+z)/151]^2 = 2.19[(1+z)/11]^2$ K since the matter and radiation temperature decouples at $z \sim 150$ and matter temperature drops as $(1+z)^{-2}$ afterwards. In the photoionized case, we assume the gas to be at a temperature 10^4 K, appropriate for a photoionized gas with primordial abundance.

In addition, we consider a third case, of that of a primordial supernova (SN) in a high redshift minihalo (z = 10–20, $M_h = 10^5$–10^7 M$_\odot$), which was discussed by Sazonov & Sunyaev (2015).

2.3.1 Gas cooling

In the case of a photoionized IGM with primordial composition, we use the cooling due to bremsstrahlung and recombination cooling (Efstathiou 1992), using the rates given in appendix A by Hui & Gnedin (1997).

For the case of neutral gas, the resulting temperature is small ($\leq$1000 K), and the cooling time exceeds the Hubble time. Therefore, gas cooling can be neglected in this case.

3 EVOLUTION OF CR SPECTRUM

The calculation of the evolution of CR spectrum and resulting heating of the gas is described next for two different cases.

3.1 Neutral IGM

In case of neutral medium, we write (5) in terms of β of the proton:

$$-\frac{\mathrm{d}\beta}{\mathrm{d}t} = 3.9\times10^{-16}\left(\frac{n_{\rm HI}}{\rm cm^{-3}}\right)\frac{\beta(1-\beta^2)^{3/2}}{\beta_c^3+2\beta^3}. \quad (8)$$

Furthermore, for a proton with diffusion coefficient D, the rms speed is given by

$$\frac{\mathrm{d}r}{\mathrm{d}t} = \frac{3D}{r}. \quad (9)$$

Combining these two equations, we have

$$\frac{\mathrm{d}\beta}{\mathrm{d}r_{\rm kpc}} = 1.2\times10^{-2}\,\frac{(n_{\rm HI}/\rm cm^{-3})\,r_{\rm kpc}}{(D/10^{29}\rm cm^2\,s^{-1})}\,\frac{\beta(1-\beta^2)^{3/2}}{\beta_c^3+2\beta^3}, \quad (10)$$

where $r_{\rm kpc}$ is the distance from the virial radius of the galaxy in kpc unit. This equation can be analytically solved to give β as a function of r, given an initial value β_0. This is given by

$$\begin{aligned}&\tan(\arcsin\beta)-(\arcsin\beta)+(\beta_c^3/2)\ln\tan\left(\frac{\arcsin\beta}{2}\right)+\\&\quad\frac{(\beta_c^3/2)}{\cos(\arcsin\beta)}\\&=\tan(\arcsin\beta_0)-(\arcsin\beta_0)+(\beta_c^3/2)\ln\tan\left(\frac{\arcsin\beta_0}{2}\right)\\&+\frac{\beta_c^3/2}{\cos(\arcsin\beta_0)}-\frac{3.1\times10^{-3}(n_{\rm HI}/\rm cm^{-3})\,r_{\rm kpc}^2}{(D/10^{29}\,\rm cm^2\,s^{-1})}. \quad (11)\end{aligned}$$

This relation can be used to trace the evolution of the CR spectrum as a function of distance r, given a density of the medium.

A useful parameter to define in this context is the distance through which the minimum energy CR proton loses all its energy, which is calculated from equation (11), using a value of β_0 corresponding to $E_{0,\rm min}$. This distance scale will be important in describing the results of temperature profile later in the paper. We have found that this length-scale r_0 can be approximately determined by

$$r_0 \approx 0.1\,\rm kpc\left(\frac{E_{0,\rm min}}{1\,\rm MeV}\right)^{0.73}\left(\frac{n_{\rm HI}}{1\,\rm cm^{-3}}\right)^{-0.54}\left(\frac{D}{10^{29}\rm cm^2 s^{-1}}\right)^{1/2}. \quad (12)$$

In the case of $z = 10$ and $\Delta = 10$, the corresponding particle density is $n_{\rm HI}\approx0.003\ \rm cm^{-3}$, and a 1 MeV proton loses all its energy within a distance $\approx$2.2 kpc from the virial radius. We will refer to these values when we discuss the effect of IGM heating.

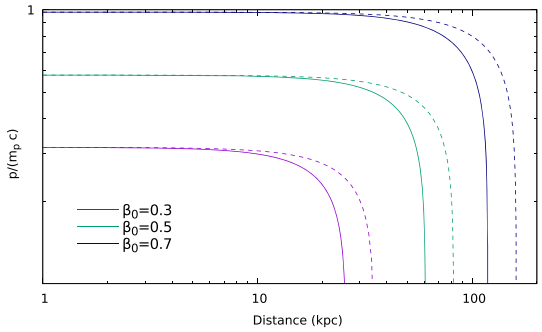

Figure 3. Change in the dimensionless momentum $p/(m_pc)$ of a proton with distance for different initial values of p (whose corresponding β_0 values are shown as labels), for $z = 10$ and $\Delta = 10$. Solid lines show the case of ionized IGM and dashed lines show the case of neutral IGM.

3.2 Photoionized IGM

In the case of photoionized gas, we can write equation (4) in terms of β as

$$-\frac{\mathrm{d}\beta}{\mathrm{d}t} = 3.3\times10^{-16}\,\rm s^{-1}\left(\frac{n_e}{\rm cm^{-3}}\right)\frac{\beta(1-\beta^2)^{3/2}}{\beta^3+x_m^3}. \quad (13)$$

For analytical simplicity, we assume x_m to be a constant and fix its value appropriate for $T = 10^4$ K. As in the case of neutral medium, we have for the evolution of β with distance

$$-\frac{\mathrm{d}\beta}{\mathrm{d}r_{\rm kpc}} = 0.01\times\frac{(n_e/\rm cm^{-3})\,r_{\rm kpc}}{(D/10^{29}\,\rm cm^2\,s^{-1})}\,\frac{\beta(1-\beta^2)^{3/2}}{\beta^3+x_m^3}. \quad (14)$$

The resulting relation between β and r for a given β_0 is given by

$$\begin{aligned}&\tan(\arcsin\beta)-(\arcsin\beta)+x_m^3\ln\tan\left(\frac{\arcsin\beta}{2}\right)+\\&\quad\frac{x_m^3}{\cos(\arcsin\beta)}\\&=\tan(\arcsin\beta_0)-(\arcsin\beta_0)+x_m^3\ln\tan\left(\frac{\arcsin\beta_0}{2}\right)\\&+\frac{x_m^3}{\cos(\arcsin\beta_0)}-5\times10^{-3}\,\frac{(n_e/\rm cm^{-3})\,r_{\rm kpc}^2}{(D/10^{29}\,\rm cm^2\,s^{-1})}. \quad (15)\end{aligned}$$

The corresponding change in momentum as a function of distance is shown in Fig. 3 for the case of $\Delta = 10$ and $z = 10$.

3.3 Change in spectrum

The loss of energy in protons changes the CR proton spectrum as they diffuse outwards from the virial radius of the parent galaxy. The CR proton spectrum at a given distance r is calculated using $n_{cr}(\beta(r))\mathrm{d}\beta = n_{cr}(\beta_0)\mathrm{d}\beta_0$, which follows from the conservation of the number of CRs. In order to evaluate it, we use the relation between β, β_0, and r from equation (11) and (15). Note that $n_{cr}(\beta)$ is related to the SFR according to the normalization equation (1) and has dimensions of time^{-1}.

We show in Fig. 4 two examples of how the CR spectrum changes at different distances from the galaxy, for the case of SFR=10 $\rm M_\odot\ yr^{-1}$, ionized IGM, (solid curves), and SFR=0.003 $\rm M_\odot\ yr^{-1}$, neutral IGM, (dashed curves) both at $z = 10$ and assuming $\Delta = 10$. As expected, we find that more and more low-energy CR protons are depleted as they diffuse outward.

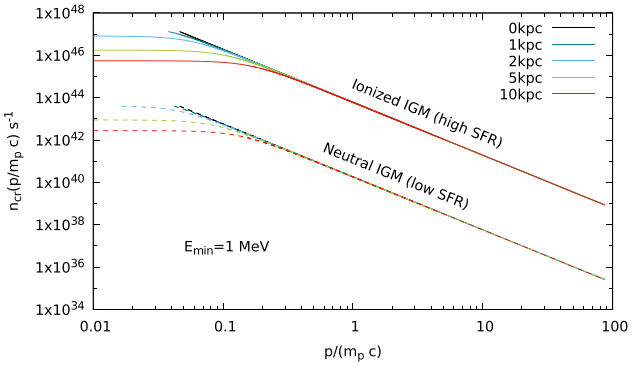

Figure 4. The spectrum of CR protons is shown at different distances by solid lines for ionized ($z = 10$ and SFR $= 10\,\mathrm{M_\odot\ yr^{-1}}$) and by dashed lines for neutral ($z = 10$ and SFR $= 0.003\,\mathrm{M_\odot\ yr^{-1}}$) medium. Both curves assume $\Delta = 10$.

4 GAS HEATING

In the case of ionized IGM, the total energy lost by CR protons goes into heating the IGM gas. However, in the case of neutral IGM, only a fraction $f_{\rm heat}$ of the energy lost by protons is used for the heating of the IGM gas, and the rest is spent in partially ionizing the neutral gas and excitation of neutral atoms. This fraction depends not only on the CR proton energy but also on secondary ionization process (by the ejected electrons). Effectively, it depends on the fractional ionization x_e of the gas. As discussed in Sazonov & Sunyaev (2015), this fraction $f_{\rm heat} \sim 0.25$ for $x_e \sim 0.01$. As a conservative estimate, we use a fraction of $f_{\rm heat} = 0.25$ for the case of neutral IGM and $f_{\rm heat} = 1$ for ionized IGM in our calculations.

The rate of increase of energy density ϵ in a spherical shell of IGM gas at distance r and width Δr due to interaction of ionized gas with a CR proton of velocity βc for a time interval of Δt can be written as

$$\frac{\mathrm{d}\epsilon}{\mathrm{d}t} = f_{\rm heat}\,\frac{\mathrm{d}E(\beta)}{\mathrm{d}t}\,\frac{1}{4\pi r^2 \Delta r}\,\Delta t\,. \tag{16}$$

Here, Δt is the residence time of a proton in this particular shell during its outward diffusion. We write this as

$$\frac{\mathrm{d}\epsilon}{\mathrm{d}t} = f_{\rm heat}\,\frac{\mathrm{d}E(\beta)}{\mathrm{d}t}\,\frac{1}{4\pi r^2 \frac{\mathrm{d}r}{\mathrm{d}t}}\,H[t - r^2/(6D)]\,, \tag{17}$$

where $\frac{\mathrm{d}r}{\mathrm{d}t}$ refers to the diffusion equation (9), and the Heavyside step function uses the arrival time ($=r^2/(6D)$) of protons at the particular shell at distance r. For an ensemble of CR protons, we integrate this over the CR spectrum at this shell, $n_{cr}(\beta)\mathrm{d}\beta$. We finally arrive at

$$\frac{\mathrm{d}\epsilon}{\mathrm{d}t} = 5\times10^{-19}\,\mathrm{erg\,s^{-1}}\,f_{\rm heat}\left(\frac{n_e}{\mathrm{cm^{-3}}}\right)\frac{1}{4\pi r^2}\sqrt{\frac{2t}{3D}} \times H[t - r^2/(6D)]\int_{\beta_{0\rm min}}^{\beta_{0\rm max}}\frac{\beta^2 n_{cr}(\beta_0)}{\beta^3 + x_m^3}\mathrm{d}\beta_0\,. \tag{18}$$

Here, we have written the CR spectrum in terms of the initial spectrum $n_{cr}(\beta_0)\mathrm{d}\beta_0 (\equiv n_{cr}(\beta)\mathrm{d}\beta)$ in order to explicitly show the limits in terms of the initial values, whose constraints have been discussed in Section 1.

In the approximation of static gas, the energy deposited by CR protons into the gas results in the change in temperature as $d\epsilon = \frac{3}{2} n_{\rm IGM} k\, dT$. However, we also take gas cooling into account in order to calculate the change in temperature with time.

4.1 Continuous SF case

We first discuss the case of continuous star formation. The process of star formation is likely to last for as long as there is gas available. The typical star formation time-scale is the inverse of the specific SFR, and it decreases from ∼10 Gyr at $z = 0$ to ∼0.3 Gyr at $z \geq 2$ (Lehnert et al. 2015). For a conservative estimate, it is reasonable to assume that CR heating continues for a time period of ∼0.1 Gyr.

The resulting temperature profiles are shown in Fig. 5 for $z = 10$ for two cases: high SFR ($10\,\mathrm{M_\odot\ yr^{-1}}$ in a $10^{10}\mathrm{M_\odot}$ galaxy) with photoionized IGM in the upper left-hand panel, and low SFR ($0.003\,\mathrm{M_\odot\ yr^{-1}}$ in a $10^{12}\mathrm{M_\odot}$ galaxy) with neutral IGM in the lower left-hand panel. Dashed lines show the temperature profile without cooling, and solid curves show the profile with cooling, for three different epochs, at 10, 50, and 100 Myr after the onset of star formation. Black curves show the result of heating with initial energy lower limit of protons at 1 MeV, and the green curves show the profiles when the lower limit is 100 keV.

The profiles show a discontinuity, which stems from the assumption of the initial spectrum being a power law down to a certain minimum energy and zero below it. The discontinuity in the temperature profile occurs at r_0 (which is given by equation 12) from the virial radius ($\mathrm{R_{vir}} = 6.4$ kpc for $10^{10}\mathrm{M_\odot}$ galaxy and $\mathrm{R_{vir}} = 29.6$ kpc for $10^{12}\mathrm{M_\odot}$ galaxy) of the source galaxy where the minimum energy proton loses all its energy, as defined earlier. In reality, the spectrum will have a smooth change of slope below the minimum energy assumed here, and the temperature profile will consequently be more continuous than shown here. However, it is useful to define the distance r_0, as we have done here, which indicates a change of shape in the temperature profile.

In the limit of static gas, the change in temperature is independent of the density, since $\mathrm{d}\epsilon (= 1.5 n_{\rm IGM} k \mathrm{d}T) \propto n_e$ in equation (18). However, the profile strongly depends on Δ since r_0 depends on gas density.

As expected from the value of the diffusion coefficient, the heating effect is noticeable only within a few kpc. This is further reduced when gas cooling is considered. We also show the variation of the result with diffusion coefficient in the middle panels, for three values of D. As expected from previous discussion, the local heating decreases with increasing value of D. We also show the variation of the results with the CR spectral index α and find that a flatter energy spectrum decreases the heating effect.

4.2 Minihalo-SF burst case

Next, we discuss the case of a burst of star formation in high redshift minihaloes, as considered by Sazonov & Sunyaev (2015). As representative cases, we consider a minihalo of total halo mass $\mathrm{M_h} = 10^6\,\mathrm{M_\odot}$ at two redshifts $z = 10$, and $z = 20$. The corresponding virial radii of the galaxy at these redshifts are $r_{\rm vir} = 0.29, 0.15$ kpc. Following Sazonov & Sunyaev (2015), we assume that the average SN explosion energy is $E_{\rm SN} = 10^{52}$–10^{53} erg and the average number of SNe per minihalo is $f_{\rm SN} = 1$. As in the previous section, we assume that a fraction $\eta = 0.1$ of the total SNe energy is converted into accelerating CR particles.

We can adopt the gas heating equation (18) to the case of a burst of CR particles, by writing $n_{cr}(\beta_0) = N_{\rm cr}(\beta_0)\delta(t - [r^2/(6D)])$ within the integral. The distribution function of CR particles produced in the burst is normalized by

$$\int E_{\rm k}\, N_{\rm cr}(p_0)\,\mathrm{d}p_0 = \eta f_{\rm SN} E_{\rm SN}\,, \tag{19}$$

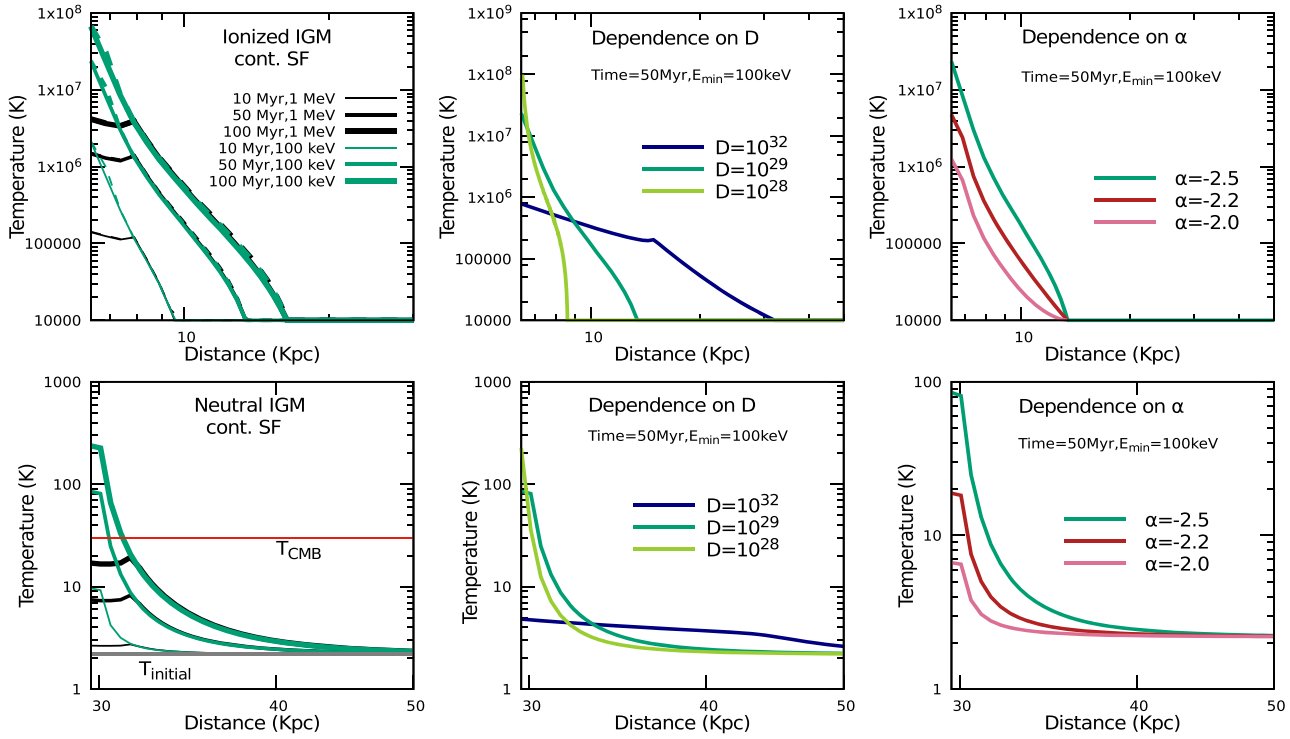

Figure 5. The temperature profile for SFR=10M$_\odot$ yr^{-1}, M$_h$ = 10^{10}M$_\odot$ (upper panel), and SFR=0.003M$_\odot$ yr^{-1}, M$_h$ = 10^{12}M$_\odot$ (lower panel) is shown for 10,50, and 100Myr at $z = 10$ using $D = 10^{29}$cm^{2}s^{-1} and $\Delta = 10$. The left-hand panels show the case of heating of photoionized gas (upper left) and neutral IGM gas (lower left). Dashed lines show the profiles without cooling and solid lines show the profiles with cooling. In the lower panels, the horizontal red line corresponds to the CMB temperature. The middle panels show the variation of the result with diffusion coefficient, and the right-hand panels show the variation with CR spectral index α.

which is similar to equation (2).

In the absence of cooling in the neutral IGM (since the resulting temperature change is shown to be small next), the CR particles heat up the surrounding as they diffuse and sweep past the IGM gas. The change in the energy density of gas at distance r at time t due to CR protons with initial β_0 is given by

$$\begin{aligned}\Delta\epsilon(r) &= \int_0^t n_{cr}(\beta_0) f_{\rm heat} \frac{{\rm d}E}{{\rm d}t} \frac{1}{4\pi r^2} \sqrt{\frac{2t}{3D}}\, {\rm d}t \\ &= \frac{1}{4\pi r^2} \int_0^t N_{\rm cr}(\beta_0)\delta[t - \frac{r^2}{6D}]\, f_{\rm heat} \frac{{\rm d}E}{{\rm d}t} \sqrt{\frac{2t}{3D}}\, {\rm d}t \\ &= \frac{2.9\times10^{-19}}{12\pi D\, r} \left(\frac{n_{\rm HI}}{\rm cm^{-3}}\right) f_{\rm heat} \frac{2\beta^2}{\beta_c^3 + 2\beta^3} N_{\rm cr}(\beta_0)\,. \end{aligned} \quad (20)$$

Here, $\frac{{\rm d}E}{{\rm d}t}$ refers to energy loss of a CR proton in neutral medium (equation 5).

The resulting temperature difference at distance r from the minihalo is found by a simple integration over the energy spectrum of CR to be

$$\Delta T = \frac{7.4\times10^{-5} f_{\rm heat}}{D\times r} \times \frac{n_{\rm HI}}{n_{\rm IGM}} \int_{\beta_{0\rm min}}^{\beta_{0\rm max}} \frac{\beta^2 N_{\rm cr}(\beta_0)}{2\beta^3 + \beta_c^3} {\rm d}\beta_0\,. \quad (21)$$

Again, the temperature profile is dependent on the assumption of Δ through the relation between β_0 and β by equation (11). We show the results in Fig. 6 for the case of $E_{\rm SN} = 10^{52}$ erg for PopIII stars and $f_{\rm SN} = 1$, at two redshifts $z = 10$, 20. The more optimistic case of a pair instability SN with $E_{\rm SN} = 10^{53}$ erg is shown by the upper curve, for which the value of ΔT is an order of magnitude larger than the fiducial case, and the IGM temperature exceeds the CMB temperature near the virial radii.The integral in the above equation is roughly constant up to a distance of r_0 from the virial radius and decreases as $r^{0.7\alpha}$ beyond that, roughly up to $\sim 2r_0$. Therefore, the temperature profile for 0.1MeV < E$_{\rm min}$ < 1MeV can be written as

$$\begin{aligned}\Delta T \approx\ & 25\,{\rm K} \left(\frac{f_{\rm heat}}{0.25}\right) \left(\frac{\eta\, f_{\rm SN}\, E_{\rm SN}}{0.1\times10^{52}\,{\rm erg}}\right) \left(\frac{E_{0,\rm min}}{1\,{\rm MeV}}\right)^{-1.2} \times \\ & \left(\frac{|\alpha|}{2.5}\right)^{10.8\times\left(\frac{E_{0,\rm min}}{1\rm MeV}\right)^{-0.1}} \times (r_{\rm kpc} + R_{\rm vir})^{-1} \times \\ & \left(\frac{D}{10^{29}\,{\rm cm^2\,s^{-1}}}\right)^{-1} \quad , R_{\rm vir} < r < (r_0 + R_{\rm vir}) \\ \Delta T \approx\ & \Delta T(r_0 + R_{\rm vir}) \left(\frac{r_{\rm kpc} + R_{\rm vir}}{r_0 + R_{\rm vir}}\right)^{[0.7\alpha-1]} \\ & , (r_0 + R_{\rm vir}) < r < (2r_0 + R_{\rm vir})\,. \end{aligned} \quad (22)$$

If the diffusion coefficient increases beyond the fiducial value at high redshift because of a lower magnitude of magnetic field in the IGM, then the temperature profile extends to larger distances but with a lower magnitude.

Fig. 6 also shows the typical distances between minihaloes ($R_{\rm interhalo}$), assuming a minimum halo mass of 10^6 M$_\odot$, with vertical arrows. We can then use our calculated temperature profile to determine the average increase in temperature within this length-scale, given by

$$\Delta T_{\rm avg} = \frac{\int \Delta T 4\pi r^2 dr}{(4/3)\pi(R^3_{\rm interhalo} - R^3_{\rm vir})}\,. \quad (23)$$

This value should be compared with the global temperature increase calculated by Sazonov & Sunyaev (2015). Following them, if we define a fraction $\eta_{\rm LECR}$ as the product of CR acceleration efficiency (η) and the energy fraction carried by low-energy CRs (which de-

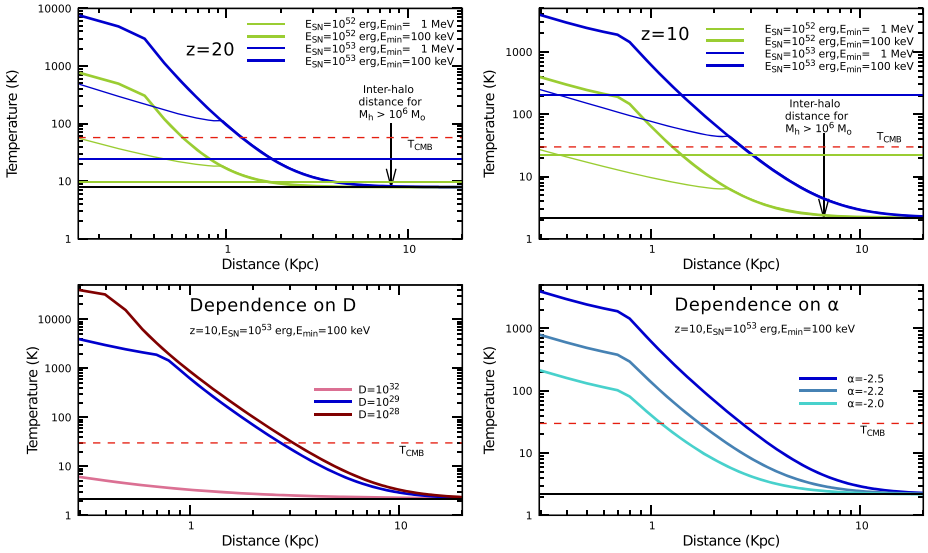

Figure 6. The temperature profile for a primordial SN in a minihalo of $M_h = 10^6$ $M_\odot$ at $z = 20$ (leftmost panel) and $z = 10$ (second from left-hand panel). The green curves in both panels show the case for $E_{SN} = 10^{52}$ erg and the blue curves, for $E_{SN} = 10^{53}$ erg; upper curves are for $E_{min} = 100$ keV and lower curves are for $E_{min} = 1$ MeV. The horizontal green and blue lines correspond to the increased global mean temperature in each case. The horizontal red dashed lines correspond to the CMB temperature. Vertical arrows mark the inter-minihalo distance for a minimum mass of 10^6 $M_\odot$. The two panels at the bottom show the variation of the result with diffusion coefficient (bottom left) and CR spectral index α (bottom right), as in Fig. 5.

posit their energy into the IGM within the Hubble time), and $n_h(z)$ as the number density of minihaloes, then according to their equation (11), the global increase in temperature is given by

$$\Delta T_{IGM} = \frac{f_{heat}\eta_{LECR} f_{SN} E_{SN}}{(3/2)k\, n_{IGM}(z)} n_h(z)\,. \quad (24)$$

We have calculated this value using the appropriate $n_h(z)$, for $M_{min} = 10^6$ $M_\odot$, $M_{max} = 10^7$ $M_\odot$, using the CAMB transfer function calculator and the fitting function of Reed et al. (2007). The calculation has been done by the HMF calculator provided by Murray, Power & Robotham (2013). The fraction η_{LECR} depends on the assumed CR spectrum, and we use the appropriate values in our calculation. For $\alpha = -2.5$, the energy fraction in low-energy CR ($\leq$30 MeV) is 0.17, and for $\alpha = -2.2$, it is 0.05. Since we have used a CR acceleration efficiency(η) of 10 per cent, we have $\eta_{LECR} = 0.017$ and 0.005 for $\alpha = -2.5$ and -2.2, respectively.

If the local average as calculated using equation (23) exceeds the global average increase in temperature, then it would imply that the heating by CR is patchy, and the temperature profiles presented here are representative of the effect of CR heating. On the other hand, if the local average is less than the global average increase in temperature, then it would mean that CR heating is rather uniform, and the temperature profile calculated by us would be subsumed under the global increase in temperature.

We find from equation (24) that for $E_{SN} = 10^{53}$erg, the global temperature increase is 198 K at redshift 10 and 16 K at redshift 20, whereas the local average temperature increase from equation (23) is 16 K and 2 K at redshift 10 and 20, respectively. Therefore, we can put upper bounds on the diffusion coefficient D at high redshift, for which CR heating would be inhomogeneous (larger D would imply a more uniform heating). We have found that at $z = 10$, the limit is $D \leq 1 \times 10^{26}$ cm^2 s^{-1}. Therefore, for our fiducial value (see Section 2.2) of $D \sim 10^{29}$ cm^2 s^{-1}, the heating is likely to be uniform. At $z \sim 20$, the corresponding limit is $D \leq 5$–6×10^{26} cm^2 s^{-1}, which also implies uniform heating since D is likely to be above this limit. However, one should remember there are uncertainties in the evolution of magnetic field with redshift and the dependence of D on the magnetic field.

4.3 Effect of a density profile

Having calculated the temperature profile using a constant IGM density, we now show the effect of a density profile by assuming a simple power-law relation. Simulations of accretion of mass around massive haloes have shown that the density profile around the virial radius of haloes is steeper than r^{-2} but becomes flatter than r^{-2} beyond the virial radius (up to a distance of $\sim 5R_{vir}$) (Prada et al. 2006). Moreover, the overdensity at $\sim R_{vir}$ is $\Delta \sim 100$. The overall profile from R_{vir} to $\sim 5R_{vir}$ can therefore be approximated by

$$n(r) = 100 \frac{\rho_{cr}(z)\Omega_m(z)\, f_b}{\mu m_p} \left(\frac{r}{R_{vir}}\right)^{-2}. \quad (25)$$

This profile would change the r-dependence in the equations relating β and β_0 (equations 11 and 15) that can be analytically calculated.

We show the change in the temperature profile for the minihalo case in Fig. 7, for $z = 10$ and $M_h = 10^6$ $M_\odot$, for two values of E_{SN} and $E_{min} = 0.1$ MeV. The dashed profiles correspond to a uniform density with $\Delta = 10$ as assumed earlier (see Fig. 6). The solid lines show the case of the above-mentioned density profile. The approximate concurrence of these two curves justifies our assumption of $\Delta = 10$ for the uniform density case.

The case of a continuously star-forming galaxy with a density profile outside R_{vir} is shown in Fig. 8. Here, although the temperature near the virial radius is similar to the case of uniform density (again justifiying the assumption of $\Delta = 10$), the temperature profile is steeper than the uniform density case because of the change in the relation between β with distance.

5 DISCUSSION

The temperature profile in the neutral case shows that if the SFR is to be low enough to keep the surrounding gas neutral and high

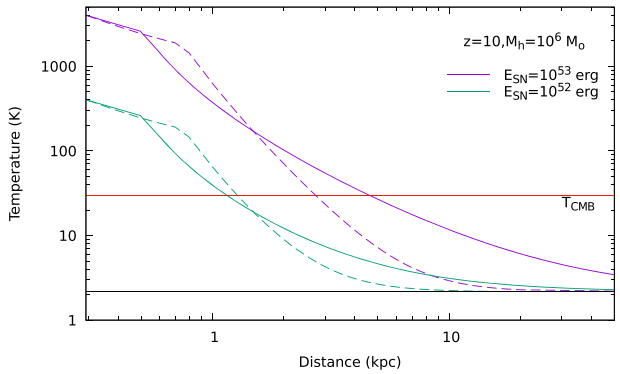

Figure 7. The temperature profile for a primordial SN in a minihalo of mass $10^6 M_\odot$ and at $z = 10$ assuming $E_{min} = 0.1$MeV. The dashed curves show the temperature profiles when the gas density outside the halo is 10 times the baryonic matter density at that epoch, and the solid curves are obtained using a density profile of gas around the halo.

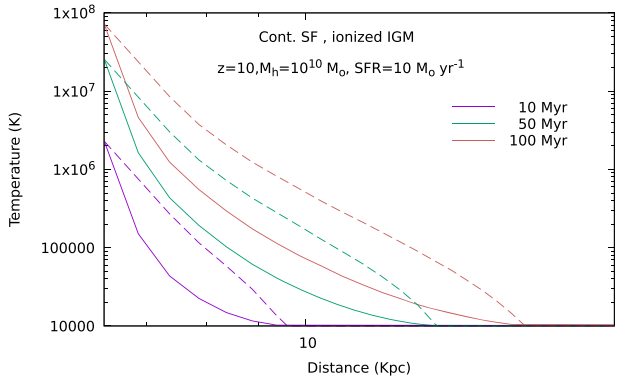

Figure 8. The temperature profile for continuous star formation in a galaxy of $M_h = 10^{10} M_\odot$ at $z = 10$ assuming $E_{min} = 0.1$ MeV. The dashed curves show the temperature profiles when the gas density outside the halo is uniform and 10 times the baryonic matter density at that epoch, and the solid curves are obtained using a density profile of gas around the halo as in equation (25).

enough to cause substantial heating, as in the case portrayed in the lower panel of Fig. 5, the gas temperature can exceed the CMB temperature (shown by a horizontal red line) within a few kpc of the galaxy, if the lower limit of CR proton energy is 100 keV. This was the scenario sketched by Sazonov & Sunyaev (2015), which we have quantified here, and shown the dependencies on various parameters.

However, even if such a case of heating arises, it is unlikely to be probed in the near future by observations as the corresponding angular scale is very small, of the order of a few arc seconds.

The temperature profiles in Fig. 5 show that gas temperature in the ionized case can increase to 10^7 (10^6) K for $E_{0,min} = 0.1(1)$ MeV in a time period of ∼50 Myr, for SFR of 10 $M_\odot$ yr^{-1}. This implies that the gas in the outskirts of the galaxy likely to be heated up to a high temperature, which would set up an outward motion. This will affect the gas infall into the parent galaxy and in turn influence the evolution of the star formation process in it.

It is reasonable to argue that if the sound speed of the gas heated by CR exceeds the infall velocity near a galaxy, then CR heating will tend to suppress the further gas infall. The infall velocity is roughly estimated as $\sqrt{GM_h/R_{vir}}$ and independent of the distance from the galaxy, up to $\sim 1.5 \times R_{vir}$ (Goerdt & Ceverino 2015). Therefore, we

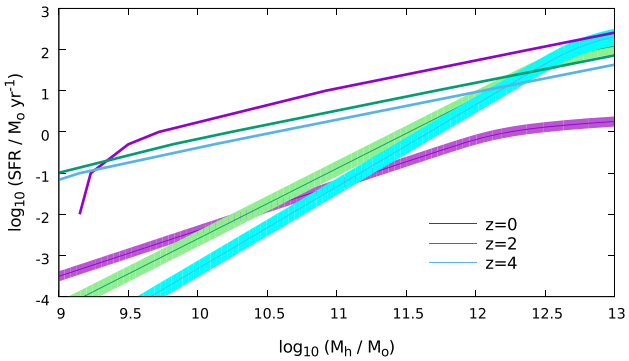

Figure 9. SFR for galaxies of different masses are shown for $z = 0$, 2, and 4. Shaded lines show the SFRs of main sequence of galaxies, and the solid lines show the lower limits of SFR from the condition that sound speed of the heated gas near the virial radius should exceed the infall speed, $E_{0,min} =$ 100 keV.

can determine the minimum SFR needed to inhibit gas infall around a galaxy of a given mass at a certain redshift. We can then compare it to the SFR of main sequence of galaxies appropriate for galaxies of same mass at that redshift.

We show in Fig. 9 the SFR of main sequence of galaxies as a function of halo mass at $z = 0$, 2, and 4 by shaded lines. We have used the fit to SFR as a function of stellar mass and cosmic time as given by Speagle et al. (2014), and the analytical fit for the relation between stellar mass and halo mass, as given by Behroozi, Conroy & Wechsler (2010), and the shaded region shows $1-\sigma$ error bars. Superposed in same figure are lines that show the lower limits on SFR needed to suppress gas infall by CR heating near the virial radius, for $E_{0,min} = 100$ keV (solid lines). For the calculation at these low redshifts, we have used a fiducial value $D = 10^{29}$cm^2 s^{-1}, as discussed in Section 2.2.

We find that, if the lower limit of CR protons is 100 keV when they escape from galaxy, then CR heating affects the infall of gas around galaxies of $M_h \sim 10^{10}$ $M_\odot$ for SFR of order ∼1 $M_\odot$ yr^{-1}. For more massive galaxies, CR heating can be important for suppression of infall if the SFR ≥100 times the SFR of main sequence of galaxies, at $z = 0$. This gap (between required SFR and SFR of main sequence of galaxies) narrows with increasing redshift. At $z \sim 4$, infall around galaxies with $M_h \sim 10^{12}$ $M_\odot$ can be affected for the SFR of main sequence of galaxies. Therefore, CR heating can be an important feedback mechanism for regulating gas infall around massive galaxies at high redshift.

6 SUMMARY

We have calculated the radial temperature profile of the IGM around galaxies due to heating by CR protons after taking into account the effect of diffusion of CRs. We assumed a simple power-law CR spectrum with a low-energy cut-off and a constant diffusion coefficient for low-energy CRs. We considered three cases: (1) heating of neutral IGM at high redshift around galaxies with low enough SFR, so that the IGM is not photoionized, (2) heating of photoionized IGM around high SFR galaxies, and (3) heating of neutral IGM at high redshift around a minihalo on account of primordial SNe. Our main results are as follows:

(i) It is not easy for low-energy CRs to escape relatively massive galaxy (Fig. 1).

(ii) The surrounding medium of galaxies at high redshift is likely to be ionized on account of star formation in the galaxy. Therefore, the heating by CRs will proceed in a different manner than previously considered case of neutral IGM heating.

(iii) In the case of CRs from minihaloes at $z \sim 10$–20, we put an upper bound on the diffusion coefficient ($D \leq 1 \times 10^{26}$ cm^2 s^{-1} for $z \sim 10$ and $D \leq 5$–6×10^{26} cm^2 s^{-1} for $z \sim 20$) for which the heating is inhomogeneous, after comparing our temperature profiles with the estimate of global temperature increase. Given the expected scaling of the diffusion coefficient with redshift, this bound suggests uniform heating, both at $z \sim 10$ and 20. But the uncertainties in CR parameters (spectrum, lower energy limit of emerging CRs, diffusion coefficient, and its dependence on magnetic field) and magnetic field at high redshift preclude any firm conclusion.

(iv) In the case of continuous star formation and neutral IGM in the vicinity of galaxies with low SFR, the temperature exceeds the CMB temperature for $D < 10^{30}$ cm^2 s^{-1}, and in this case, the profile is too peaked to be detectable.

(v) Furthermore, we found that the heated gas near the virial radii of galaxies can provide a feedback mechanism by inhibiting the infall of gas, especially for massive galaxies at high redshift ($z \sim 4$), and low-mass star-forming galaxies at low redshifts for sufficiently high SFR.

ACKNOWLEDGEMENTS

We would like to thank an anonymous referee for invaluable comments and P. L. Biermann, S. Biswas, P. Sharma, and Y. Shchekinov for valuable discussions.

REFERENCES

Behroozi P. S., Conroy C., Wechsler R. H., 2010, ApJ, 717, 379
Caprioli D., Spitkovski A., 2014, ApJ, 783, 91
Efstathiou G., 1992 MNRAS, 256, 43L
Ginzburg V. L., Ozernoi L. M., 1966, Sov. Astron., 9, 726
Goerdt T., Ceverino D., 2015, MNRAS, 450, 3359
Lacki B. C., 2015, MNRAS, 448, 20L
Lam H., Gnedin N. Y., 1997, MNRAS, 292, 27
Lehnert M. D., van Driel W., Le Tiran L., Di Matteo P., Haywood M., 2015, A&A, 469, 416
Leite N., Evoli C., D'Angelo M., Ciardi B., Sigl G., Ferrara A., 2017, MNRAS, 577, 112
Mannheim K., Schlickeiser R., 1994, A&A, 286, 983
Murray S. G., Power C., Robotham A. S. G., 2013, Astron. Comput., 3, 23
Nath B. B., Biermann P. L., 1993, MNRAS, 265, 241
Nath B. B., Madau P., Silk J., 2006, MNRAS, 366, L35
Nath B. B., Gupta N., Biermann P. L., 2012, MNRAS, 425, L86
Planck Collaboration XVI, 2015, 571, 16
Prada F., Klypin A. A., Simonneau E., Betancort-Rijo J., Patiri S., Gottlöber S., Sanchez-Conde M. A., 2006, ApJ, 645, 1001
Ptuskin V., 2012, Astropart. Phys., 39, 44
Ptuskin V., Moskalenko I. V., Jones F. C., Strong A. W., Zirakashvili V. N., 2009, ApJ, 642, 902
Reed D. S., Bower R., Frenk C. S., Jenkins A., Theuns T., 2007, 12, 379
Sazonov S., Sunyaev R., 2015, MNRAS, 454, 3464
Speagle J. S., Steinhardt C. L., Capak P. L., Silverman J. D., 2014, ApJS, 214, 15
Subramanian K., 2016, Rep. Prog. Phys, 79, 1

This paper has been typeset from a TEX/LATEX file prepared by the author.